Earth and Planetary Science Letters 434 (2016) 298–307

Contents lists available at ScienceDirect

Earth and Planetary Science Letters

www.elsevier.com/locate/epsl

Impacts of dust reduction on the northward expansion of the African monsoon during the Green Sahara period

Francesco S.R. Pausata [a,*,1], Gabriele Messori [a,1,2], Qiong Zhang [b]

[a] Department of Meteorology, Stockholm University and Bolin Centre for Climate Research, Stockholm, Sweden
[b] Department of Physical Geography, Stockholm University and Bolin Centre for Climate Research, Stockholm, Sweden

ARTICLE INFO

Article history:
Received 1 September 2015
Received in revised form 20 November 2015
Accepted 27 November 2015
Available online 14 December 2015
Editor: D. Vance

Keywords:
African Humid Period
vegetation–dust feedbacks
West African Monsoon

ABSTRACT

The West African Monsoon (WAM) is crucial for the socio-economic stability of millions of people living in the Sahel. Severe droughts have ravaged the region in the last three decades of the 20th century, highlighting the need for a better understanding of the WAM dynamics. One of the most dramatic changes in the West African Monsoon (WAM) occurred between 15000–5000 yr BP, when increased summer rainfall led to the so-called "Green Sahara" and to a reduction in dust emissions from the region. However, model experiments are unable to fully reproduce the intensification and geographical expansion of the WAM during this period, even when vegetation over the Sahara is considered. Here, we use a fully coupled simulation for 6000 yr BP (Mid-Holocene) in which prescribed Saharan vegetation and dust concentrations are changed in turn. A closer agreement with proxy records is obtained only when both the Saharan vegetation changes and dust decrease are taken into account. The dust reduction strengthens the vegetation–albedo feedback, extending the monsoon's northern limit approximately 500 km further than the vegetation-change case only. We therefore conclude that accounting for changes in Saharan dust loadings is essential for improving model simulations of the WAM during the Mid-Holocene.

1. Introduction

Following the devastating droughts that ravaged the Sahel in the 1970–1980s, many efforts have been directed at investigating climate variability in Northern Africa, focusing on vegetation–climate feedbacks and the dynamics of the West African Monsoon (WAM) system (Charney et al., 1975; Giannini et al., 2003). However, the past millennia have witnessed much larger precipitation changes than those seen in recent decades. One of the most dramatic changes in the WAM began around 15000 yr BP, when increased summer precipitation led to an expansion of the North African lakes and wetlands. Grassland and shrubland covered areas that are currently desert (Holmes, 2008), giving origin to the so-called "Green Sahara", or African Humid Period. The African Humid Period ended between ~5500 and ~4000 yr BP (Armitage et al., 2015; deMenocal et al., 2000; Shanahan et al., 2015; Weldeab et al., 2007). Climate model simulations for the Mid-Holocene (MH, 6000 yr BP) are not currently able to fully reproduce the intensification and geographical expansion of the African monsoon (Harrison et al., 2014). Hargreaves et al. (2013) have shown that this is not a function of the resolution at which the data-model comparisons are made, and that the source of these discrepancies must lie in a shortcoming common to all models.

The Paleoclimate Modelling Intercomparison Project/Coupled Model Intercomparison Project (PMIP/CMIP) protocols assume the MH to have the same dust concentrations and land cover as the pre-industrial period (Taylor et al., 2009). However, paleo-proxy data indicate that dust emissions during the MH were 70–80% lower than today (Arbuszewski et al., 2013; deMenocal et al., 2000; McGee et al., 2013), and the Sahara desert was replaced to a great extent by shrubs and grassland (Holmes, 2008). The key to the models' dry bias may therefore be an incorrect representation of vegetation and dust concentrations. On the one hand, several studies have already shown that variations in vegetation and soil type can have a major impact on precipitation, similar in magnitude to that induced by orbital forcing (e.g., Braconnot et al., 1999, 2000; Chikira et al., 2006; Claussen and Gayler, 1997; Claussen et al., 1998; Krinner et al., 2012; Kutzbach and Liu, 1997; Kutzbach et al., 1996). Nevertheless, the precipitation increase due to land cover changes alone is not sufficient to correct the models' dry bias, revealing only partial agreement with the most recent paleo-data records (Harrison et al., 2014; Krinner et al., 2012; Lézine et al., 2011; Shanahan et al., 2015). On the other hand, there

* Corresponding author.
E-mail address: francesco.pausata@misu.su.se (F.S.R. Pausata).
[1] The authors have equally contributed to the manuscript.
[2] Current affiliation: Met Office Hadley Centre, Exeter, UK.

http://dx.doi.org/10.1016/j.epsl.2015.11.049

Table 1
Albedo and leaf area index (LAI) for desert, evergreen shrub and grassland/steppe and the domain over which the vegetation changes are applied in each set-up.

Vegetation type		Albedo	LAI	Domain
PS	Mainly desert	0.30	0.18	11°–33°N 15°W–35°E
		0.29	0.28	23°–33°N 15°E–35°E
GS	Evergreen shrub	0.15	2.6	11°–33°N 15°W–35°E
GS2	Evergreen shrub	0.15	2.6	11°–22°N 15°W–35°E
				23°–33°N 15°W–14°E
	Grassland/steppe	0.25	1.0	23°–33°N 15°E–35°E

are yet no estimates of the potential impacts of Saharan dust reduction on the MH WAM. Changes in mineral dust loading can alter both incoming solar radiation and cloud properties (DeMott et al., 2003); they can further lead to changes in atmospheric and oceanic circulation (e.g., Evan et al., 2006; Serra et al., 2014; Wang et al., 2012), precipitation, storm development and sea surface temperatures (SSTs) (Booth et al., 2012; Evan et al., 2011, 2009). This points to dust as the potential gap in our current understanding of past WAM changes.

Here we use climate model simulations to examine the relative importance of vegetation and Saharan dust concentrations in affecting the MH WAM strength and in driving the associated atmospheric circulation changes. Our primary goal is to understand and quantify the role of dust reduction under a vegetated Sahara.

2. Model description and experimental set-up

2.1. The model

The present study uses the latest version of the fully coupled global climate model EC-Earth (version 3.1, Hazeleger et al., 2010). The atmospheric model is based on the Integrated Forecast System (IFS cycle 36r4) developed by the European Centre for Medium-range Weather Forecasts, including the H-TESSEL land model. The simulation is run at T159 horizontal spectral resolution (roughly 1.125°) with 62 vertical levels. The atmospheric component is coupled to the Nucleus for European Modelling of the Ocean version 2 (NEMO, Madec, 2008), developed at the Institute Pierre Simon Laplace, and the Louvain-la-Neuve Sea Ice Model version 3 (LIM3, Vancoppenolle et al., 2008). The coupling is performed by the OASIS 3 coupler (Valcke, 2006). The ocean component NEMO has a nominal horizontal resolution of 1° and 46 vertical levels. The EC-Earth version used in this study has prescribed vegetation. The aerosol concentrations are provided as prescribed fields. The aerosol indirect effects are not included in the model version used in this study. The annual cycle of the various aerosol types follows Tegen et al. (1997). A detailed description of the aerosol components can be found in Hess et al. (1998). In Table S1 we report the characteristics of the dust particles in our model.

2.2. Experiments set-up

We use as reference scenario the climate of the MH, with insolation and greenhouse gas concentrations from 6000 yr BP. Differences in the Earth's orbit in the MH enhanced the amplitude of the seasonal cycle in Northern Hemisphere insolation by ~5% compared to present day values. In the control MH simulation (MH_{CNTRL}), we impose PI dust concentrations and vegetation over the Sahara (desert), as described in the CMIP5 protocol (Taylor et al., 2009). While it is well established that dust mobilization during the mid-Holocene was lower compared to the late Holocene, we follow the protocol to ease the comparison of our results to the literature. We also simulate the PI climate to validate the model and assess the impact of the orbital forcing alone (see Supplementary material). We then perform an idealized experiment ($MH_{GS\text{-}RD}$) in which the vegetation type over the Sahara (11°–33°N and 15°W–35°E) is set to shrub, typical of the modern Sudanian Savanna ecoregion, and the PI dust amount is reduced by up to 80% (Fig. S1), based on recent estimates of Saharan dust flux reduction during the MH (Arbuszewski et al., 2013; deMenocal et al., 2000; McGee et al., 2013). A recent model simulation using an atmospheric-aerosol model with an embedded scheme to detect potential dust sources has confirmed this massive dust emission reduction during the Mid-Holocene (Egerer et al., 2015). The vegetation change corresponds to a reduction in the surface albedo from ~0.3 to 0.15 over the Sahara region and an increase in the leaf area index from ~0.2 to 2.6 (desert and shrub respectively; Table 1). The dust reduction leads to a decrease in the global dust aerosol optical depth (AOD) of almost 60% and in the total AOD of 0.02 (Fig. 1 and Table S1). Finally, we perform two further experiments in which the pre-industrial Saharan dust concentrations and vegetation are changed in turn ($MH_{*S\text{-}*D}$).

The idealized set-up of the experiments enables a better investigation of the role of dust under a vegetated Sahara. Furthermore, recent proxy studies have shown that, during the African Humid Period, paleo-lakes extended at least up to 28°N (Lézine et al., 2011) and Sudanian Savanna type vegetation (dominated by shrubs) was centered between 20° and 25°N and reached as far as 28°N – about 6–9° latitude further north than the modern distribution (Hély et al., 2014). An earlier and commonly adopted vegetation reconstruction (Hoelzmann et al., 1998) does not account for such an extensive greening, instead prescribing steppe vegetation north of 20°N. In view of the above, the idealized vegetation cover in our sensitivity experiments may not be entirely unrealistic, especially in the Western Sahara. We have nonetheless tested the sensitivity of our results to the choice of the vegetation cover by performing an additional set of experiments in which the shrubland is replaced by grassland (steppe) over the eastern Sahara domain ($MH_{GS2\text{-}*D}$).

It is difficult to verify whether the imposed vegetation cover and dust reduction are consistent with one another without a fully interactive aerosol scheme. Nevertheless, the dust-scaling factor is based on proxy evidence and the imposed vegetation cover is consistent – in particular in the $MH_{GS2\text{-}*D}$ experiments – with the inferred large increase in precipitation, as discussed in Sections 3.4 and 4.

The details of the boundary conditions for the sensitivity experiments are listed in Table 2. Initial conditions were taken from a 700-year pre-industrial spin-up run, and the simulations were then run for approximately 300 yr. The climate reaches quasi-equilibrium after 100 to 200 yr, depending on the experiment. In this paper we focus on the equilibrium responses, and only the last 100 yr of each sensitivity experiment are analyzed.

2.3. Monsoon diagnostics

In order to quantify the impacts of Saharan dust and vegetation on the WAM, we define the onset, duration and northernmost

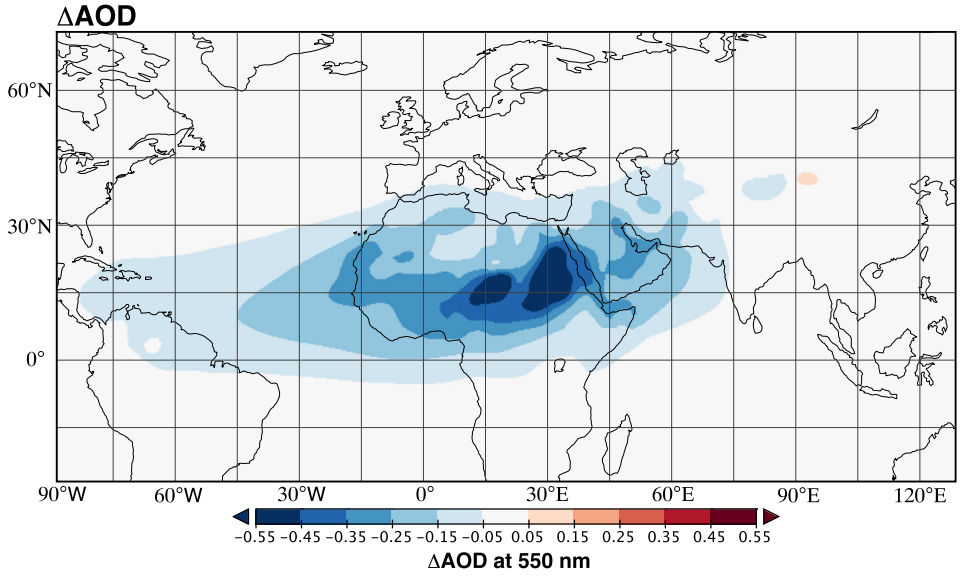

Fig. 1. *Dust-induced changes in AOD.* Annual mean changes in AOD at 550 nm between the pre-industrial and the reduced dust concentrations. (For interpretation of the colors in this figure, the reader is referred to the web version of this article.)

Table 2
Boundary conditions for all MH experiments.

Simulation	Orbital forcing years BP	GHGs	Saharan vegetation	Saharan dust
MH_{CNTRL}	6000	MH	desert	PI
$MH_{GS\text{-}PD}$	6000	MH	shrub	PI
$MH_{GS2\text{-}PD}$	6000	MH	shrub/steppe	PI
$MH_{PS\text{-}RD}$	6000	MH	desert	Reduced
$MH_{GS\text{-}RD}$	6000	MH	shrub	Reduced
$MH_{GS2\text{-}RD}$	6000	MH	shrub/steppe	Reduced

extent of the monsoon. These three metrics are computed over the same zonal domain, spanning 15°W–20°E. A range of different domains are used in the literature to diagnose the monsoon's duration and extent, ranging from relatively narrow cases (e.g. 10°W–10°E, Sultan and Janicot, 2003), to much wider domains (e.g. 20°W–22.5°E, Zhang and Cook, 2014). Here, we chose an intermediate extent. To test the robustness of our results, the onset, duration and geographical extent diagnostics were repeated for a 10°W–10°E domain, and the qualitative conclusions drawn in the paper were unaffected.

The monsoon's onset is defined as the date preceding the largest increase in precipitation over a 20-day period at the latitude of the maximum in the first EOF of the zonally averaged rainfall (Sultan and Janicot, 2003). The withdrawal is defined as the date on which the zonally averaged precipitation at the same latitude falls below 2 mm/day, for at least 20 consecutive days. The duration is then simply the time intervening between the onset and withdrawal dates. Finally, the northernmost extent of the monsoon is defined as the northernmost latitude where the zonally averaged rainfall exceeds 60 mm/month. This is consistent with the 2 mm/day threshold adopted for defining the monsoon's withdrawal. Full details of the three metrics are provided in the Supplementary material.

3. Results

3.1. The mid-Holocene control

The MH_{CNTRL} simulation displays a WAM starting in late June and lasting for approximately four months (Table S2), with peak precipitation values reaching over 16 mm/day on the western coastline of Guinea and Sierra-Leone and almost 11 mm/day in the interior (Fig. 2b). These values slightly exceed present-day observations (cf. Fig. 2 and Fig. S6), in agreement with the behavior of most CMIP5 models (Harrison et al., 2014). The northernmost extent of the monsoon is just above 16°N (Fig. 2b, Table 3), 2° latitude further north than in the PI simulation. The climatological June–September (JJAS) surface temperatures range from slightly under 40 °C in the Western Sahara to 20 °C on the coastline of the Gulf of Guinea (Fig. 2a). This represents a warming of the Saharan domain and a cooling of Equatorial Africa compared to PI conditions, and again follows closely the behavior of most CMIP5 models (Harrison et al., 2014).

3.2. The Green Sahara-reduced dust scenario

Changing the land cover from desert to shrub and reducing the dust concentrations ($MH_{GS\text{-}RD}$) leads to a wide-ranging increase in climatological JJAS precipitations, together with a significant change in surface temperatures across the domain (Fig. 2c). The peak intensification in precipitation occurs in the Sahel, with local increases exceeding 9 mm/day. The signal extends across the Sahara, with increases of 1–2 mm/day on the Mediterranean coastline (Fig. 2d). On the opposite, the wet coastal regions in Equatorial Africa see local reductions in excess of 5 mm/day. The northernmost boundary of the monsoon reaches approximately 30°N, roughly 1500 km north of the control case (Fig. 2d and Table 3). This shift is accompanied by an extension of the wet season by about one and a half months, from late May to early November (Table S2).

Such a strong precipitation change can be traced back to the decreased surface albedo over North Africa – owing to the vegetation changes – and the increased incoming shortwave radiation at the surface – owing to the reduced dust concentrations

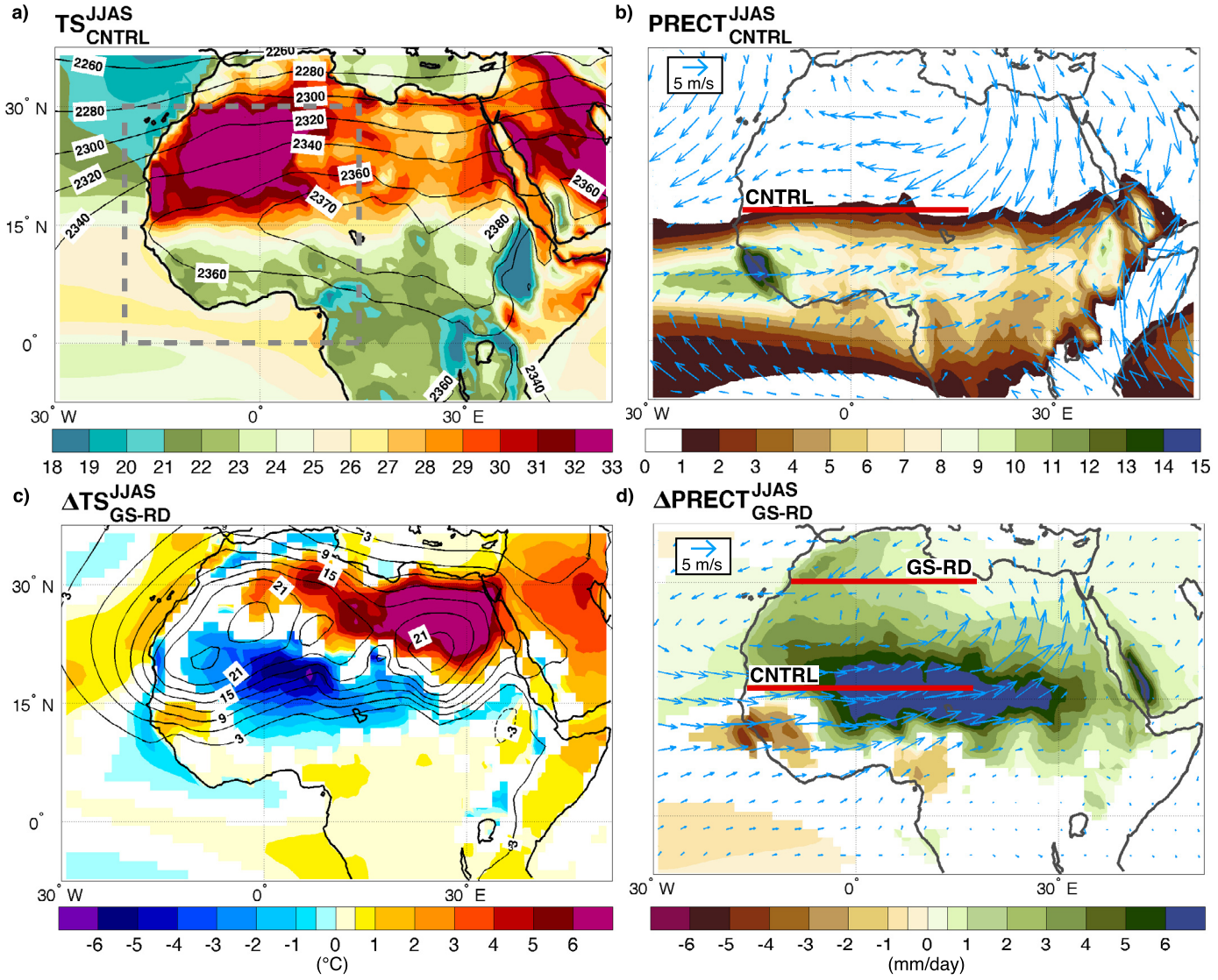

Fig. 2. *Summer averaged surface temperature, lower atmospheric thickness, low-level wind and precipitation in the MH_{CNTRL} and $MH_{GS\text{-}RD}$ changes.* MH_{CNTRL} summer (JJAS, June to September) climatological values of surface temperature (°C, shadings) (a); precipitation (mm/day, shadings) and 850 hPa wind (m/s, vectors) (b); and pre-monsoon (MAM, March to May) lower atmospheric thickness (m, contours) (a). $MH_{GS\text{-}RD}$ changes relative to MH_{CNTRL} in surface temperature and lower atmospheric thickness (c); and in precipitation and 850 hPa wind (d). The box in (a) marks the Western Saharan domain. The horizontal lines in (b) and (d) mark the maximum northward extent of the WAM in the two experiments. Only differences significant at the 99% confidence level using a *t* test are shaded in (c) and (d). (For interpretation of the colors in this figure, the reader is referred to the web version of this article.)

Table 3
Monsoon's northernmost extent for all experiments.

Simulation	Extent
MH_{CNTRL}	16.3°N
$MH_{GS\text{-}PD}$	26.4°N
$MH_{PS\text{-}RD}$	16.3°N
$MH_{GS\text{-}RD}$	30.8°N
$MH_{GS2\text{-}PD}$	27.5°N
$MH_{GS2\text{-}RD}$	30.8°N
PI	14.0°N

(Fig. S2). These two elements lead to a strong warming over the Sahara in the months preceding the monsoon (Fig. S3b). This, in turn, drives an intensification of the Saharan heat low, here diagnosed as the difference between the 700 and 925 hPa geopotential heights (Lavaysse et al., 2009) (also termed as lower atmospheric thickness, Fig. 2c and see Supplementary material). The intensified Saharan low (i.e. increased atmospheric thickness) favors a northward shift of the convection during the monsoon onset. Once the wet season starts, the impact of latent heat changes dominates the temperature signal, leading to a cooling of 5 °C or more across most of the Sahel (Fig. 2c). Beyond the range of the monsoon, in the eastern portion of the domain, the albedo signal outweighs the latent heat changes throughout the summer, leading to an intense warming locally exceeding 7 °C. A tripolar SST anomaly pattern also develops over the ocean, with a warming in the north tropical and equatorial Atlantic and a localized cooling in between, coinciding with decreased precipitations off the coast of Guinea (Fig. 2c). At the same time, anomalous westerlies develop across the Sahel (Fig. 2d), driving an increase in moisture over the continent (Fig. S4b, see also Cook and Vizy, 2006). At upper levels, this westerly anomaly leads to a weakening and a northward shift of the African Easterly Jet (Fig. S5b). Similar SST and wind anomaly patterns have previously been linked to enhanced Sahelian precipitations (Cook, 1999; Kutzbach and Liu, 1997), and a greater penetration of the monsoonal flow over the continent (Cook, 1999).

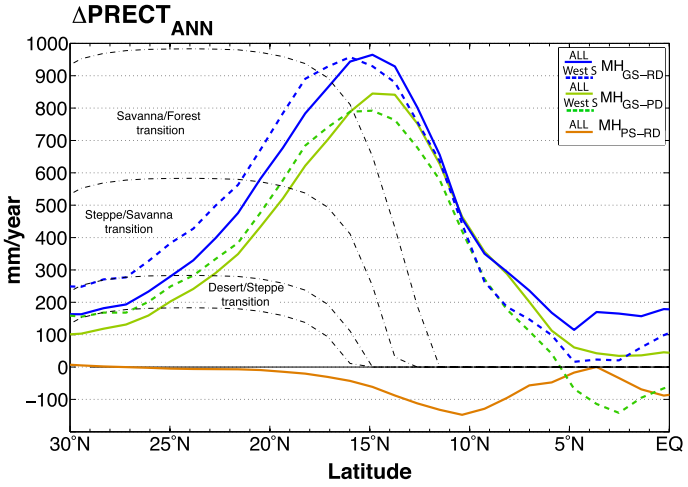

Fig. 3. *Annual mean precipitation anomalies and ecoregion transition thresholds.* Annual mean precipitation anomalies over land relative to MH_{CNTRL}. The dash–dot lines indicate the precipitation increases necessary for the transition between different ecoregions, based on present day climate conditions. The precipitation values are zonally averaged over the entire Northern Africa (solid lines, 20°W–30°E) and over the Western Sahara (dashed lines), corresponding to the region where the precipitation anomalies are always above the Desert/Steppe transition. The ecoregions are defined based on Olson et al. (2001) and correspond to Sahelian Acacia Savanna (Steppe), Sudanian Savanna (Savanna) and Guinean Forest–Savanna Mosaic (Forest). (For interpretation of the colors in this figure, the reader is referred to the web version of this article.)

The vegetation over the Sahara also increases precipitation through the insolation–monsoon–vegetation feedback (e.g, Braconnot et al., 1999; Kutzbach and Liu, 1997). A broader vegetation cover enhances the water vapor flux and the latent heating of the atmosphere, amplifying the amount of rainfall for a given insolation change. However, the latter effect has a marginal influence compared to the albedo feedback of vegetation cover (Hales et al., 2004).

3.3. The respective roles of dust and vegetation

To further illuminate the linkages between changes in land cover and dust boundary conditions and WAM intensity, an additional set of sensitivity experiments is carried out in which pre-industrial Saharan dust concentrations and vegetation are changed in turn (MH_{*S-*D}, Table 2). Any differences between the MH_{CNTRL} and the sensitivity experiments (MH_{*S-*D}) must be due to either the greening of the Sahara, the dust reduction, or their combined effect.

We find that the vegetation albedo (MH_{GS-PD}) drives about 65–70% of the increase in WAM strength (Figs. 3 and 4b), leading to both a lengthening of the monsoon season (Table S2) and a northward shift of the WAM's boundary to over 26°N (Fig. 4b; Table 3). The anomalies in surface temperature, lower atmospheric thickness, humidity and wind in the MH_{GS-PD} scenario resemble those of the MH_{GS-RD}, albeit generally weaker (cf. Figs. 2c, d, S3b, S4b, S5b and 4a, b, S3c S4c, S5c). These changes drive an intensification of the monsoon following similar dynamical mechanisms to the ones discussed above.

Notwithstanding the large effect of vegetation in our simulation, the northern limit of the monsoon in the MH_{GS-PD} simulation is significantly further south (about 500 km) than in the MH_{GS-RD} case. The dust reduction under a vegetated Sahara enhances local precipitation from 0.5 to 2.5 mm/day (Fig. 5c), increasing the annual rainfall over the Western Sahara by 100–200 mm/yr north of 15°N (Fig. 3). The Steppe/Savanna transition in the MH_{GS-PD} simulation only extends up to 24°N over the Western Sahara, 6° latitude further south than in the MH_{GS-RD} case.

Dust reduction under vegetated Sahara conditions therefore has a major impact on the WAM: to put this into perspective, the northward shift due to the dust is about twice as large as the shift due to the changes in orbital forcing between the PI and MH_{CNTL} experiments, with the former accounting for ∼4° latitude and the latter for ∼2° latitude change (Table 3).

In stark contrast to its effects under vegetated Sahara, the dust reduction alone (MH_{PS-RD}) does not lead to any precipitation increase over the Sahara and Sahel regions. On the opposite, it triggers a decrease in precipitation over the Sahel, locally reaching 1.5 mm/day (Figs. 3, 4d). The dust reduction over a desert Sahara has little influence on the planetary albedo, thus leading to no significant direct thermal forcing at the surface in the pre-monsoon months (Figs. S2c and S3d). The Sahel instead experiences a significant surface warming owing to the darker surface compared to the desert (Figs. 4c and S3d), which in turn increases the lower atmospheric thickness to the south of the climatological heat low. This may then favor the enhanced easterly flow seen in the summer (JJAS) months, which advects dry air across the continent and weakens the monsoonal precipitations (Figs. 4d, S4d, S5d). An additional driver of the reduction in Sahelian precipitation may be the indirect dust-SST feedback. The decreased dust concentrations favor a warming of the Arabian Sea and tropical Atlantic SSTs (Fig. 4c). Previous studies have shown that positive SST anomalies over these ocean basins may lead to Sahelian droughts (Bader and Latif, 2003; Hoerling et al., 2006; Lu and Delworth, 2005). Finally, the decreased rainfall over the Sahel simulated in the MH_{PS-RD} experiment is also consistent with the "heat pump" theory proposed by Lau et al. (2009), whereby the dust layers warm the air over West Africa, enhance deep convection and strengthen the WAM. Reducing dust concentrations would then lead to a weakening of the "heat pump" effect and hence a decrease in rainfall. Our results indeed suggest that the decreased dust concentrations – while warming the surface over the Sahel – cool the middle and upper troposphere (Fig. S2), suggesting a waning of the "heat pump" effect. Furthermore, the "heat pump" effect is sensitive to the single scattering albedo (ω_0) of the dust particles and is most effective for highly to moderately absorbing dust ($\omega_0 < 0.95$ (Lau et al., 2009; Solmon et al., 2008)), as is the case in EC-Earth ($\omega_0 = 0.89$ at 550 nm). The strong dependence on the single scattering albedo suggests that the "heat pump" effect in climate simulations is highly dependent on model parameterization (cf. Lau et al., 2009 and Yoshioka et al., 2007). Nevertheless, under Green Sahara conditions (MH_{GS-RD}), the simulated precipitation changes indicate that the reduced "heat pump", and most likely the model-dependent response linked to dust parameterization, are overwhelmed by the surface warming associated with the underlying changes in albedo.

Our current model version does not include the aerosol indirect effect; however, we deem this effect not to be able to affect the overall conclusion of this study: the crucial changes in surface albedo and hence warming must take place in the pre-monsoonal season when no clouds are present over the Sahara. Nevertheless, the aerosol indirect effect may play a relevant role in affecting the simulated length of the monsoon season.

3.4. Sensitivity to prescribed vegetation cover

The design of the MH experiments is idealized in order to better elucidate and disentangle the respective roles of land surface cover and atmospheric dust loading in altering the large-scale circulation. To test the sensitivity of our results to the exact choice of the vegetation cover, we perform another set of experiments (MH_{GS2-RD} and MH_{GS2-PD}, Table 2) in which the shrub in the eastern Sahara (23°–33°N 15°E–35°E, grey box in Fig. 5b) is replaced with grassland/steppe vegetation type (albedo = 0.25 and

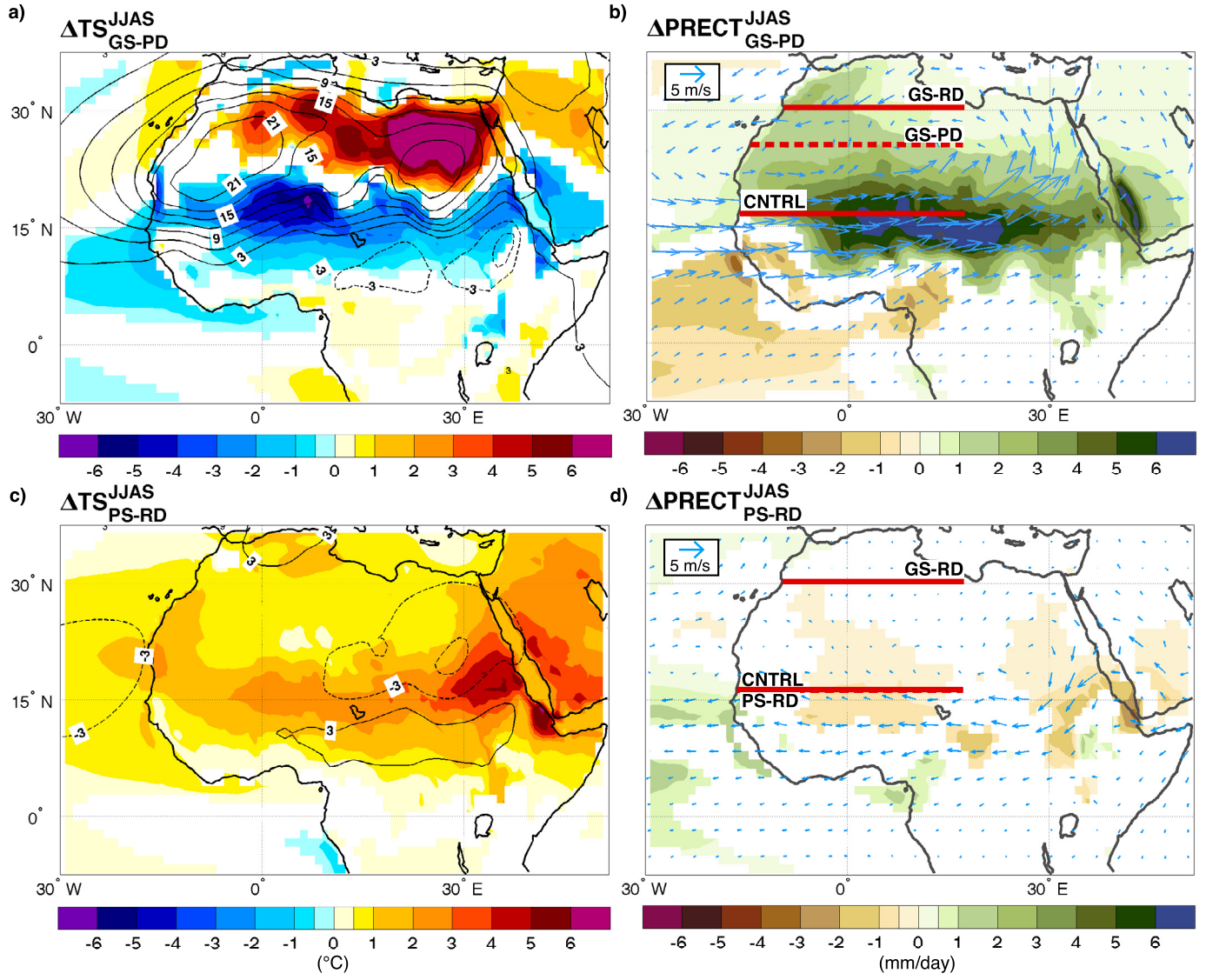

Fig. 4. *Changes in surface temperature, lower atmospheric thickness, precipitation and low-level wind in the sensitivity experiments.* Changes in summer (JJAS) mean surface temperature (°C, shadings) and in pre-monsoon (MAM) mean lower atmospheric thickness (m, contours) for $MH_{GS\text{-}PD}$ (a) and $MH_{PS\text{-}RD}$ (c) relative to the MH_{CNTRL} experiment; changes in summer mean precipitation (mm/day, shadings) and 850 hPa wind (m/s, vectors) for $MH_{GS\text{-}PD}$ (b), and $MH_{PS\text{-}RD}$ (d) relative to the MH_{CNTRL} experiment. The horizontal lines in (b) and (d) mark the maximum northward extent of the WAM in each experiment. Only differences significant at the 99% confidence level using a *t* test are shaded. (For interpretation of the colors in this figure, the reader is referred to the web version of this article.)

LAI = 1.0). This is motivated by the fact that the eastern part of the Sahara receives relatively little precipitation even under $MH_{GS\text{-}RD}$ conditions (Fig. 2d), and might not have been able to sustain an extensive shrub cover (e.g. Chikira et al., 2006; Claussen and Gayler, 1997). The eastern Sahara domain is selected as the region where the annual precipitation was below the Steppe/Savanna transition (i.e. where shrub type vegetation cannot be sustained). The precipitation in Western part of the domain, where we retain the shrub cover, never falls below the latter transition zone. A more systematic investigation of whether the rainfall increase could sustain our imposed vegetation cover would require further simulations adopting an interactive land-surface scheme, which we deem beyond the scope of this paper. Nonetheless, our idealized experiment setup is broadly consistent, with the transition bands described in Fig. 3.

The new vegetation cover results in similar atmospheric circulation (cf. Figs. 2d and 4b to 5a and 5b), temperature (cf. Figs. 2c and 4a to 6a and 6b) and precipitation changes (Fig. 5c and d) relative to the MH_{CNTRL}. The precipitation anomalies in the $MH_{GS2\text{-}*D}$ experiments are larger than for the $MH_{GS\text{-}*D}$ cases (Fig. 5c and d). In particular, the GS2 set-up leads to an even greater effect of dust on the rainfall enhancement; however, an analysis of the reasons behind this difference is beyond the scope of this paper. These additional experiments confirm the role of dust under vegetated Sahara: the greening of the Sahara drives a very strong intensification and northward extension of the WAM, and the dust reduction again accounts for an additional shift of several hundred kilometers (Fig. 5b and Table 3).

4. Discussions

4.1. Comparison to proxy records

The idealized nature of our experiments does not allow a quantitative assessment of the model results. However, the model–proxy comparison can provide useful insights on both the model performance and proxy weaknesses and strengths. As our main term of comparison, we adopt the synthesis of the pollen-based continental precipitation reconstructions in Harrison et al. (2014)

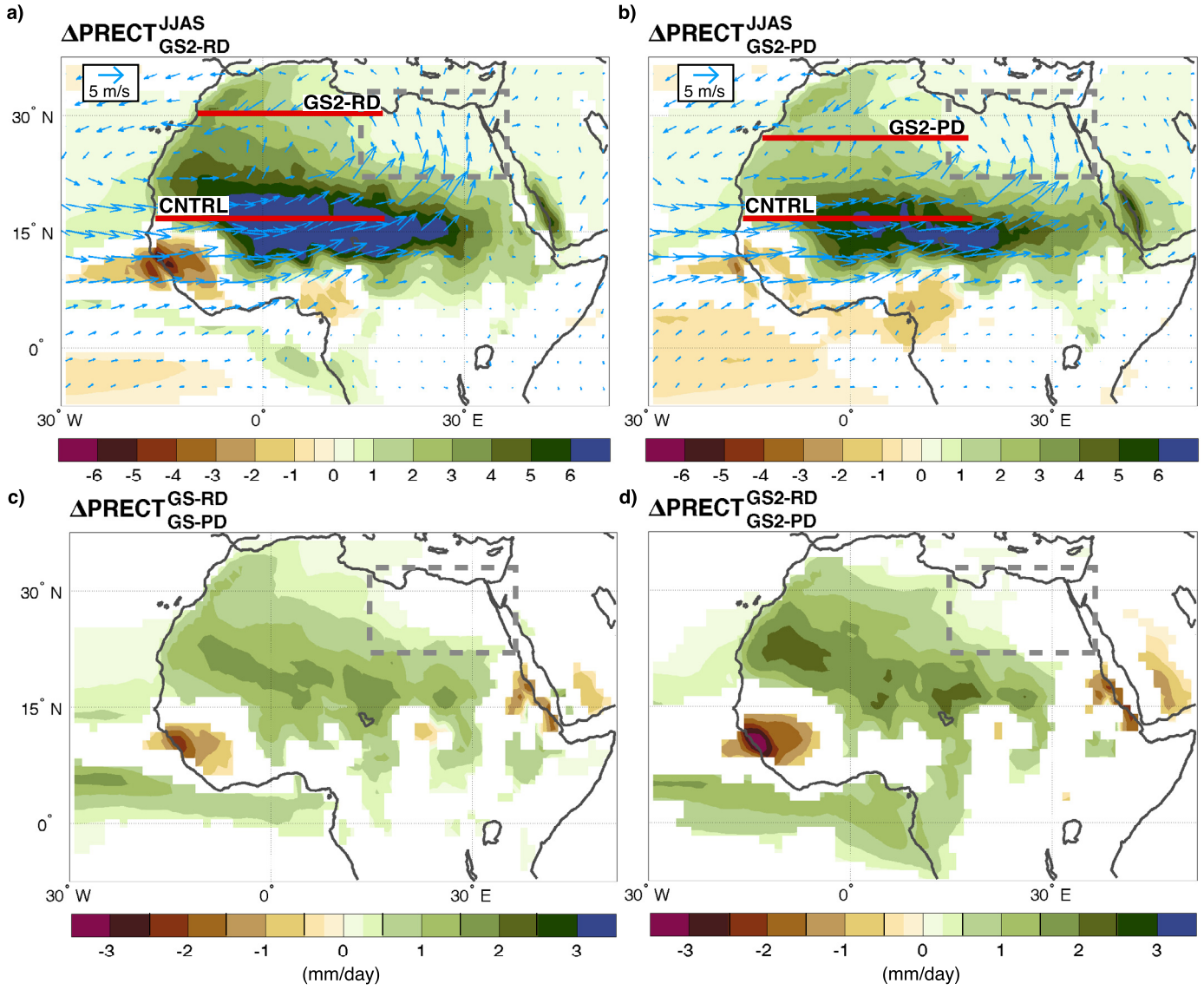

Fig. 5. *Changes in precipitation and low-level wind in the GS2 sensitivity experiments and rainfall enhancement due to dust reduction under vegetated Sahara.* Changes in summer (JJAS) mean precipitation (mm/day, shadings) and 850 hPa wind (m/s, vectors) for $MH_{GS2\text{-}RD}$ (a), and $MH_{GS2\text{-}PD}$ (b) relative to the MH_{CNTRL} experiment. Changes in summer mean precipitation between the $MH_{GS\text{-}RD}$ and $MH_{GS\text{-}PD}$ (c) and $MH_{GS2\text{-}RD}$ and $MH_{GS2\text{-}PD}$ (d) experiments. The dashed box represents the eastern Sahara domain over which shrubland was substituted by grassland/steppe. Only differences significant at the 99% confidence level using a *t* test are shaded. (For interpretation of the colors in this figure, the reader is referred to the web version of this article.)

(Fig. 7). The model data used in the comparison are taken from the $MH_{GS2\text{-}RD}$ experiment, which, within our idealized framework, has the most realistic vegetation cover.

The simulated precipitation anomalies relative to present day show a very good agreement with the proxy reconstructions (Fig. 7). The model appears to significantly overestimate the increase in MH precipitation only between 10 and 15°N. However, the latest proxy data for the African Humid Period suggest a northward shift of tropical vegetation by approximately 6–9° latitude compared to the present day location: between 25–28°N the vegetation was dominated by Sahelian (grasses) elements; between 20–25°N there was a co-occurrence of Sahelian and Sudanian Savanna (shrubs) vegetation type and the tropical rain-belt was centered between 15°–20°N (Hély et al., 2014). Therefore, an increase of about 1000 mm around 15°N does not seem unrealistic: the present day precipitation climatology ranges between 200 and 600 mm/yr at 10–15°N, whereas the region under the ITCZ receives at least 1200–1600 mm/yr.

Other datasets provide evidence that Northern Chad (Ounianga region ~20°N) received an annual rainfall of around 250 mm (Kröpelin et al., 2008), that paleo-lakes extended at least as far as 28°N, and that the WAM may have reached 30°N (Lézine et al., 2011; Shanahan et al., 2015). These records are consistent with the simulated annual rainfall over Northern Chad (~350 mm/yr) and across the Western Sahara (20°W–15°E) in the $MH_{GS^*\text{-}RD}$ experiments, which allows the Steppe/Savanna transition to extend all the way up to 30°N (Figs. 2d, 3). On the other hand, records from the Gulf of Guinea indicate an enhanced riverine runoff (e.g., Weldeab et al., 2007) that may seem at odds with the local precipitation decreases along the West African coastline. However, the Niger river has a very extensive watershed, which was probably connected to lake Chad's watershed during the MH (Lézine et al., 2005). It is therefore likely that the widespread precipitation increase across the watershed overshadowed the local decreases along the coastline, leading to an overall enhanced riverine runoff.

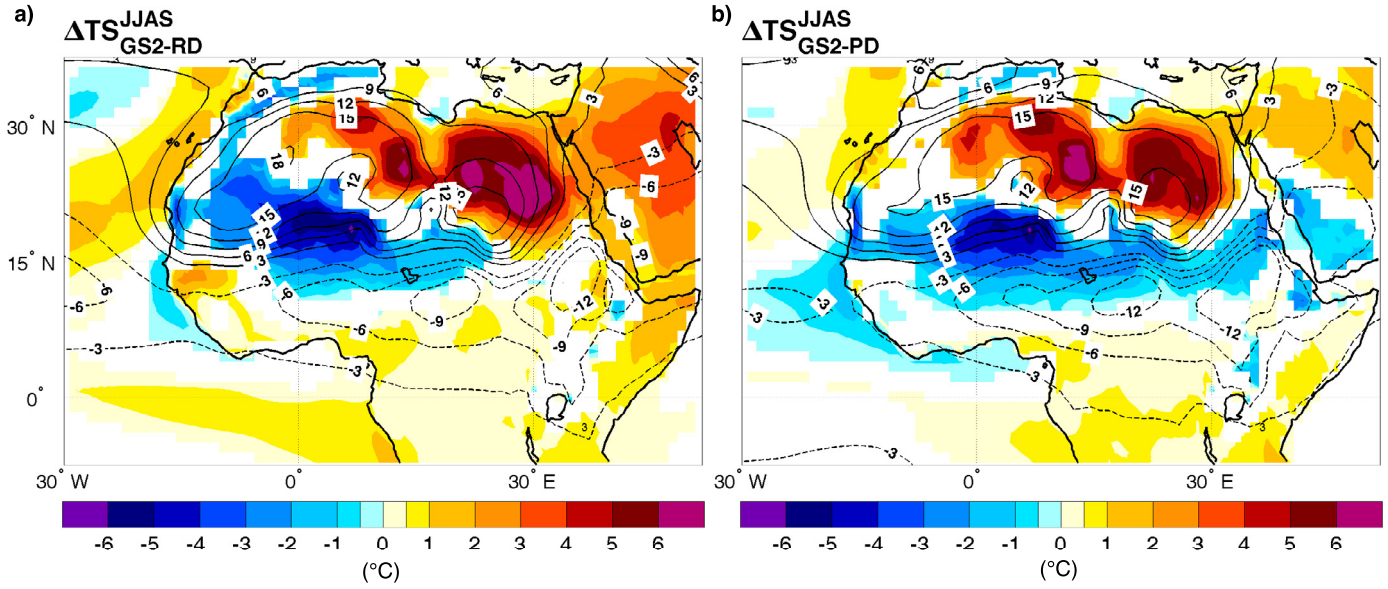

Fig. 6. *Changes in surface temperature and lower atmospheric thickness, precipitation in the GS2 sensitivity experiments.* Summer (JJAS) changes in surface temperature (°C, shadings) and in pre-monsoon (MAM, March to May) lower atmospheric thickness (m, contours) for the $MH_{GS2\text{-}RD}$ (a) and $MH_{GS2\text{-}PD}$ (b) experiments relative to the MH_{CNTRL} simulation. Only differences significant at the 99% confidence level using a *t* test are shaded. (For interpretation of the colors in this figure, the reader is referred to the web version of this article.)

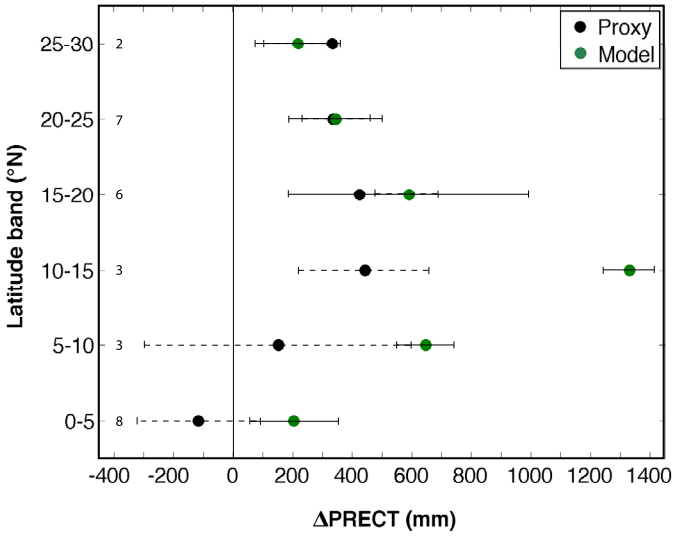

Fig. 7. *Comparison of reconstructed and simulated precipitation changes.* Zonal mean (20°W–40°E) anomalies between the MH and present day for simulated ($MH_{GS2\text{-}RD}$) and reconstructed mean annual precipitation over Northern Africa, averaged over 5° latitude bands between 0° and 30°N. The black dots represent the reconstructions from the data set in Harrison et al. (2014), which are provided as a 2° × 2° grid cell (Fig. S7) and are calculated averaging the individual site-based reconstructions within that grid cell. Twice the standard error of the mean (~95% confidence level) of the grid cell reconstructions (dotted) and the model (solid) is shown for each latitude band. The model results are averages of model output sampled at the location of the grid cells with reconstructions. The number of grid cells available for the reconstructions is shown on the plot. The present day precipitation for the model comparison is taken from the Global Precipitation Climatology Project (GPCP) Combined Precipitation Data Set Version 2.2 provided by the NOAA/OAR/ESRL PSD (http://www.esrl.noaa.gov/psd/) (Adler et al., 2003). (For interpretation of the colors in this figure, the reader is referred to the web version of this article.)

4.2. Comparison to other modeling studies

The large rainfall enhancement seen in the $MH_{GS^*\text{-}PD}$ experiments is within the range of other Green Sahara modeling studies. Among the studies using prescribed vegetation, Texier et al. (2000) simulated a zonally uniform increase in rainfall, with similar rates over the 15–20°N latitude band compared to our study, but lower values in the upper Western Sahara. A later paper by Chikira et al. (2006) prescribed the vegetation following Hoelzmann et al. (1998), thus setting the northern limit of tropical vegetation remarkably further south than what has been suggested by recent proxy studies (cf. Plate 1 in Hoelzmann et al., 1998 and Hély et al., 2014). Nevertheless, the study showed a larger precipitation increase than our $MH_{GS\text{-}PD}$ experiment (cf. Fig. 4b with Fig. 8c in Chikira et al., 2006).

Studies using climate models coupled to a dynamical vegetation also present a broad range of results. For example, Claussen and Gayler (1997) and Renssen et al. (2006) found very strong precipitation increases due to the greening of the Sahara – respectively ~50% and ~25% greater than in our study ($MH_{GS\text{-}PD}$). Claussen and Gayler (1997) simulated a mean June-to-August precipitation of 129 mm/month (over 10°W–30°E and 15°N–30°N); while in our simulation the mean precipitation in the same domain is ~86 mm/month. Furthermore, their MH reference experiment was twice as wet as our MH_{CNTL} simulation. Renssen et al. (2006) showed an increase in rainfall over the Western Sahara (14°W–3°E) of approximately 45–50 mm/month around 26–27°N, whereas in our simulation ($MH_{GS\text{-}PD}$) the increase is around 38 mm/month. In Levis et al. (2004), the rainfall increase is remarkably smaller in the equatorial region (up to 15°N) compared to our study ($MH_{GS\text{-}PD}$), nevertheless the WAM penetrates further north than in the $MH_{GS\text{-}PD}$ experiments when considering vegetation and soil feedbacks (cf. Fig. 3 with Fig. 1 in Levis et al., 2004). At the opposite end of the spectrum, other works show weaker precipitation enhancements (e.g., Braconnot et al., 1999; De Noblet-Ducoudre et al., 2000) compared to the present study. In particular, the most recent simulations performed with HadGEM2-ES and MIROC-ESM, which included both a dynamic vegetation and dust emissions, were not able to reproduce a comparable strengthening of the African monsoon (Harrison et al., 2015). Those simulations were submitted to the CMIP5 initiative and the initial configuration for the vegetation was therefore set to pre-industrial levels. The simulated MH changes in both models do not allow vegetation to grow above 15°N (see simulated precipitation anomalies in Fig. 2 in Harrison et al., 2015). Hence, the associated variations in dust load compared to pre-industrial

climate are most likely limited, and so are the feedbacks. Further studies from other modeling groups are needed to investigate how much the response to the change in dust concentrations is model-dependent.

5. Conclusions

In this study, we use a set of idealized experiments to investigate the role played by vegetation and dust concentration changes in the Sahara region in influencing the paleo-WAM. While the role of land cover in intensifying the WAM has already been documented in the literature (e.g., Braconnot et al., 1999; Chikira et al., 2006; Claussen and Gayler, 1997; Kutzbach et al., 1996), the role of dust under Green-Sahara conditions was hitherto unexplored. Under a vegetated Sahara, the WAM extends 10° latitude further north than for the desert Sahara case, reaching about 26°N. The dust reduction in the Green-Sahara set-up drives an additional rainfall increase of 0.5–2.5 mm/day across the Sahara (Fig. 5c and d) and contributes to about one third (∼500 km) of the total northward shift of the WAM. Such shift is twice as large as that due to changes in orbital forcing alone (Table 3 and cf. Figs. 2 and S6). We therefore show the importance of reduced dust concentrations in significantly enhancing the monsoon's intensity and extent under a vegetated Sahara.

Our results further highlight that changes in dust loading are crucial for improving the models' ability to simulate the MH WAM. The momentous precipitation changes seen in our study can be attributed to the unrealistic land surface cover and aerosol loading assumptions made in the CMIP5 protocol, on which the MH_{CNTL} simulation is based. This underlines the serious limitations of CMIP5 experiments in simulating the MH WAM.

These conclusions are also relevant when looking into the future, since dust emissions may decrease owing to both direct and indirect anthropogenic impacts on land cover (Mahowald and Luo, 2003). Moreover, all the Green Sahara experiments display strong westerly low-level flow anomalies (Figs. 2c, 3b, and S5) and a very wet Western Sahara contrasted by a much drier Eastern Sahara (Figs. 2d and 4a). These patterns are qualitatively similar to the anomalies observed in 21st century projections which take into account the effect of anthropogenic CO_2 emissions (Biasutti, 2013; Monerie et al., 2013).

The devastating socio-economic effects of recent droughts in the Sahel have highlighted the need for skillful long-term climate forecasts. However, the failure of most models to reproduce past WAM changes suggests that similar shortcomings might hamper simulations of future changes in Northern African rainfall.

Author contributions

F.S.R.P. conceived and designed the study. G.M. performed the dynamical analysis. F.S.R.P. and G.M. interpreted the model results and wrote the manuscript. Q.Z. carried out the model experiments, contributed to the interpretation of the model results and edited the manuscript.

Acknowledgements

The authors would like to thank D.S. Battisti for helpful discussions, and P. Braconnot, L. Garcia-Carreras, M. Gaetani and three anonymous reviewers for insightful comments on the manuscript. This work was supported by the Swedish National Space Board project Dnr 88/11. The climate model simulations and analysis were performed on resources provided by the Swedish National Infrastructure for Computing (SNIC) at NSC and Cray XC30 HPC systems at ECMWF. G. Messori is funded by Sweden's Vetenskapsrådet, as part of the MILEX project.

Appendix A. Supplementary material

Supplementary material related to this article can be found online at http://dx.doi.org/10.1016/j.epsl.2015.11.049.

References

Adler, R.F., Huffman, G.J., Chang, A., Ferraro, R., Xie, P.-P., Janowiak, J., Rudolf, B., Schneider, U., Curtis, S., Bolvin, D., Gruber, A., Susskind, J., Arkin, P., Nelkin, E., 2003. The version-2 Global Precipitation Climatology Project (GPCP) monthly precipitation analysis (1979–present). J. Hydrometeorol. 4, 1147–1167. http://dx.doi.org/10.1175/1525-7541(2003)004<1147:TVGPCP>2.0.CO;2.

Arbuszewski, J.A., deMenocal, P.B., Cléroux, C., Bradtmiller, L., Mix, A., 2013. Meridional shifts of the Atlantic intertropical convergence zone since the Last Glacial Maximum. Nat. Geosci. 6, 959–962. http://dx.doi.org/10.1038/ngeo1961.

Armitage, S.J., Bristow, C.S., Drake, N.A., 2015. West African monsoon dynamics inferred from abrupt fluctuations of Lake Mega-Chad. Proc. Natl. Acad. Sci. USA 112 (28), 8543–8548. http://dx.doi.org/10.1073/pnas.1417655112.

Bader, J., Latif, M., 2003. The impact of decadal-scale Indian Ocean sea surface temperature anomalies on Sahelian rainfall and the North Atlantic Oscillation. Geophys. Res. Lett. 30, 2169. http://dx.doi.org/10.1029/2003GL018426.

Biasutti, M., 2013. Forced Sahel rainfall trends in the CMIP5 archive. J. Geophys. Res., Atmos. 118, 1613–1623. http://dx.doi.org/10.1002/jgrd.50206.

Booth, B.B.B., Dunstone, N.J., Halloran, P.R., Andrews, T., Bellouin, N., 2012. Aerosols implicated as a prime driver of twentieth-century North Atlantic climate variability. Nature 484, 228–232. http://dx.doi.org/10.1038/nature10946.

Braconnot, P., Joussaume, S., Marti, O., de Noblet, N., 1999. Synergistic feedbacks from ocean and vegetation on the African Monsoon response to Mid-Holocene insolation. Geophys. Res. Lett 26 (16), 2481–2484. http://dx.doi.org/10.1029/1999GL006047.

Braconnot, P., Marti, O., Joussaume, S., Leclainche, Y., 2000. Ocean feedback in response to 6 kyr BP insolation. J. Climate 13, 1537–1553. http://dx.doi.org/10.1175/1520-0442(2000)013<1537:OFIRTK>2.0.CO;2.

Charney, J., Stone, P.H., Quirk, W.J., 1975. Drought in the Sahara: a biogeophysical feedback mechanism. Science 187, 434–435. http://dx.doi.org/10.1126/science.187.4175.434.

Chikira, M., Abe-Ouchi, A., Sumi, A., 2006. General circulation model study on the Green Sahara during the mid-Holocene: an impact of convection originating above boundary layer. J. Geophys. Res. 111, D21103. http://dx.doi.org/10.1029/2005JD006398.

Claussen, M., Gayler, V., 1997. The greening of the Sahara during the mid-Holocene: results of an interactive atmosphere–biome model. Glob. Ecol. Biogeogr. Lett. 6, 369. http://dx.doi.org/10.2307/2997337.

Claussen, M., Brovkin, V., Ganopolski, A., Kubatzki, C., Petoukhov, V., 1998. Modelling global terrestrial vegetation–climate interaction. Philos. Trans. R. Soc. Lond. B, Biol. Sci. 353, 53–63. http://dx.doi.org/10.1098/rstb.1998.0190.

Cook, K.H., 1999. Generation of the African easterly jet and its role in determining West African precipitation. J. Climate 12, 1165–1184. http://dx.doi.org/10.1175/1520-0442(1999)012<1165:GOTAEJ>2.0.CO;2.

Cook, K.H., Vizy, E.K., 2006. Coupled model simulations of the West African monsoon system: twentieth- and twenty-first-century simulations. J. Climate 19, 3681–3703. http://dx.doi.org/10.1175/JCLI3814.1.

De Noblet-Ducoudre, N., Claussen, M., Prentice, C., 2000. Mid-Holocene greening of the Sahara: first results of the GAIM 6000 year BP Experiment with two asynchronously coupled atmosphere/biome models. Clim. Dyn. 16, 643–659. http://dx.doi.org/10.1007/s003820000074.

deMenocal, P., Ortiz, J., Guilderson, T., Adkins, J., Sarnthein, M., Baker, L., Yarusinsky, M., 2000. Abrupt onset and termination of the African Humid Period. Quat. Sci. Rev. 19, 347–361. http://dx.doi.org/10.1016/S0277-3791(99)00081-5.

DeMott, P.J., Sassen, K., Poellot, M.R., Baumgardner, D., Rogers, D.C., Brooks, S.D., Prenni, A.J., Kreidenweis, S.M., 2003. African dust aerosols as atmospheric ice nuclei. Geophys. Res. Lett. 30, 1732. http://dx.doi.org/10.1029/2003GL017410.

Egerer, S., Claussen, M., Reick, C., Stanelle, T., 2015. Marine sediment records as indicator for the changes in Holocene Saharan landscape: simulating the dust cycle. Clim. Past Discuss. 11, 5269–5306. http://dx.doi.org/10.5194/cpd-11-5269-2015.

Evan, A.T., Dunion, J., Foley, J.A., Heidinger, A.K., Velden, C.S., 2006. New evidence for a relationship between Atlantic tropical cyclone activity and African dust outbreaks. Geophys. Res. Lett. 33, L19813. http://dx.doi.org/10.1029/2006GL026408.

Evan, A.T., Vimont, D.J., Heidinger, A.K., Kossin, J.P., Bennartz, R., 2009. The role of aerosols in the evolution of tropical North Atlantic Ocean temperature anomalies. Science 324, 778–781. http://dx.doi.org/10.1126/science.1167404.

Evan, A.T., Foltz, G.R., Zhang, D., Vimont, D.J., 2011. Influence of African dust on ocean–atmosphere variability in the tropical Atlantic. Nat. Geosci. 4, 762–765. http://dx.doi.org/10.1038/ngeo1276.

Giannini, A., Saravanan, R., Chang, P., 2003. Oceanic forcing of Sahel rainfall on interannual to interdecadal time scales. Science 302, 1027–1030. http://dx.doi.org/10.1126/science.1089357.

Hales, K., Neelin, J.D., Zeng, N., 2004. Sensitivity of tropical land climate to leaf area index: role of surface conductance versus albedo. J. Climate 17, 1459–1473. http://dx.doi.org/10.1175/1520-0442(2004)017<1459:SOTLCT>2.0.CO;2.

Hargreaves, J.C., Annan, J.D., Ohgaito, R., Paul, A., Abe-Ouchi, A., 2013. Skill and reliability of climate model ensembles at the Last Glacial Maximum and mid-Holocene. Clim. Past 9, 811–823. http://dx.doi.org/10.5194/cp-9-811-2013.

Harrison, S.P., Bartlein, P.J., Brewer, S., Prentice, I.C., Boyd, M., Hessler, I., Holmgren, K., Izumi, K., Willis, K., 2014. Climate model benchmarking with glacial and mid-Holocene climates. Clim. Dyn. 43, 671–688. http://dx.doi.org/10.1007/s00382-013-1922-6.

Harrison, S.P., Bartlein, P.J., Izumi, K., Li, G., Annan, J., Hargreaves, J., Braconnot, P., Kageyama, M., 2015. Evaluation of CMIP5 palaeo-simulations to improve climate projections. Nat. Clim. Change 5, 735–743. http://dx.doi.org/10.1038/nclimate2649.

Hazeleger, W., Severijns, C., Semmler, T., Ştefănescu, S., Yang, S., Wang, X., Wyser, K., Dutra, E., Baldasano, J.M., Bintanja, R., Bougeault, P., Caballero, R., Ekman, A.M.L., Christensen, J.H., van den Hurk, B., Jimenez, P., Jones, C., Kållberg, P., Koenigk, T., McGrath, R., Miranda, P., Van Noije, T., Palmer, T., Parodi, J.A., Schmith, T., Selten, F., Storelvmo, T., Sterl, A., Tapamo, H., Vancoppenolle, M., Viterbo, P., Willén, U., 2010. EC-Earth: a seamless Earth-system prediction approach in action. Bull. Am. Meteorol. Soc. 91, 1357–1363. http://dx.doi.org/10.1175/2010BAMS2877.1.

Hély, C., Lézine, A.-M., contributors, A., 2014. Holocene changes in African vegetation: tradeoff between climate and water availability. Clim. Past 10, 681–686. http://dx.doi.org/10.5194/cp-10-681-2014.

Hess, M., Koepke, P., Schult, I., 1998. Optical properties of aerosols and clouds: the software package OPAC. Bull. Am. Meteorol. Soc. 79, 831–844. http://dx.doi.org/10.1175/1520-0477(1998)079<0831:OPOAAC>2.0.CO;2.

Hoelzmann, P., Jolly, D., Harrison, S.P., Laarif, F., Bonnefille, R., Pachur, H.-J., 1998. Mid-Holocene land-surface conditions in northern Africa and the Arabian Peninsula: a data set for the analysis of biogeophysical feedbacks in the climate system. Glob. Biogeochem. Cycles 12, 35–51. http://dx.doi.org/10.1029/97GB02733.

Hoerling, M., Hurrell, J., Eischeid, J., Phillips, A., 2006. Detection and attribution of twentieth-century Northern and Southern African rainfall change. J. Climate 19, 3989–4008. http://dx.doi.org/10.1175/JCLI3842.1.

Holmes, J.A., 2008. Ecology. How the Sahara became dry. Science 320, 752–753. http://dx.doi.org/10.1126/science.1158105.

Krinner, G., Lézine, A.-M., Braconnot, P., Sepulchre, P., Ramstein, G., Grenier, C., Gouttevin, I., 2012. A reassessment of lake and wetland feedbacks on the North African Holocene climate. Geophys. Res. Lett. 39, L07701. http://dx.doi.org/10.1029/2012GL050992.

Kröpelin, S., Verschuren, D., Lézine, A.-M., Eggermont, H., Cocquyt, C., Francus, P., Cazet, J.-P., Fagot, M., Rumes, B., Russell, J.M., Darius, F., Conley, D.J., Schuster, M., von Suchodoletz, H., Engstrom, D.R., 2008. Climate-driven ecosystem succession in the Sahara: the past 6000 years. Science 320, 765–768. http://dx.doi.org/10.1126/science.1154913.

Kutzbach, J., Bonan, G., Foley, J., Harrison, S.P., 1996. Vegetation and soil feedbacks on the response of the African monsoon to orbital forcing in the early to middle Holocene. Nature 384, 623–626. http://dx.doi.org/10.1038/384623a0.

Kutzbach, J.E., Liu, Z., 1997. Response of the African monsoon to orbital forcing and ocean feedbacks in the middle Holocene. Science 80 (278), 440–443. http://dx.doi.org/10.1126/science.278.5337.440.

Lau, K.M., Kim, K.M., Sud, Y.C., Walker, G.K., 2009. A GCM study of the response of the atmospheric water cycle of West Africa and the Atlantic to Saharan dust radiative forcing. Ann. Geophys. 27, 4023–4037. http://dx.doi.org/10.5194/angeo-27-4023-2009.

Lavaysse, C., Flamant, C., Janicot, S., Parker, D.J., Lafore, J.P., Sultan, B., Pelon, J., 2009. Seasonal evolution of the West African heat low: a climatological perspective. Clim. Dyn. 33, 313–330.

Levis, S., Bonan, G.B., Bonfils, C., 2004. Soil feedback drives the mid-Holocene North African monsoon northward in fully coupled CCSM2 simulations with a dynamic vegetation model. Clim. Dyn. 23, 791–802. http://dx.doi.org/10.1007/s00382-004-0477-y.

Lézine, A.-M., Duplessy, J.-C., Cazet, J.-P., 2005. West African monsoon variability during the last deglaciation and the Holocene: evidence from fresh water algae, pollen and isotope data from core KW31, Gulf of Guinea. Palaeogeogr. Palaeoclimatol. Palaeoecol. 219, 225–237. http://dx.doi.org/10.1016/j.palaeo.2004.12.027.

Lézine, A.-M., Hély, C., Grenier, C., Braconnot, P., Krinner, G., 2011. Sahara and Sahel vulnerability to climate changes, lessons from Holocene hydrological data. Quat. Sci. Rev. 30, 3001–3012. http://dx.doi.org/10.1016/j.quascirev.2011.07.006.

Lu, J., Delworth, T.L., 2005. Oceanic forcing of the late 20th century Sahel drought. Geophys. Res. Lett. 32, L22706. http://dx.doi.org/10.1029/2005GL023316.

Madec, G., 2008. NEMO ocean engine. Note du Pole de modlisation, vol. 27. Institut Pierre-Simon Laplace (IPSL), Paris, France. ISSN 1288-1618.

Mahowald, N.M., Luo, C., 2003. A less dusty future? Geophys. Res. Lett. 30. http://dx.doi.org/10.1029/2003GL017880.

McGee, D., deMenocal, P.B., Winckler, G., Stuut, J.B.W., Bradtmiller, L.I., 2013. The magnitude, timing and abruptness of changes in North African dust deposition over the last 20,000 yr. Earth Planet. Sci. Lett. 371–372, 163–176. http://dx.doi.org/10.1016/j.epsl.2013.03.054.

Monerie, P.-A., Roucou, P., Fontaine, B., 2013. Mid-century effects of climate change on African monsoon dynamics using the A1B emission scenario. Int. J. Climatol. 33, 881–896. http://dx.doi.org/10.1002/joc.3476.

Olson, D.M., Dinerstein, E., Wikramanayake, E.D., Burgess, N.D., Powell, G.V.N., Underwood, E.C., D'amico, J.A., Itoua, I., Strand, H.E., Morrison, J.C., Loucks, C.J., Allnutt, T.F., Ricketts, T.H., Kura, Y., Lamoreux, J.F., Wettengel, W.W., Hedao, P., Kassem, K.R., 2001. Terrestrial ecoregions of the world: a new map of life on Earth. Bioscience 51, 933. http://dx.doi.org/10.1641/0006-3568(2001)051[0933:TEOTWA]2.0.CO;2.

Renssen, H., Brovkin, V., Fichefet, T., Goosse, H., 2006. Simulation of the Holocene climate evolution in Northern Africa: the termination of the African Humid Period. Quat. Int. 150, 95–102. http://dx.doi.org/10.1016/j.quaint.2005.01.001.

Serra, N., Martínez Avellaneda, N., Stammer, D., 2014. Large-scale impact of Saharan dust on the North Atlantic Ocean circulation. J. Geophys. Res., Oceans 119, 704–730. http://dx.doi.org/10.1002/2013JC009274.

Shanahan, T.M., McKay, N.P., Hughen, K.A., Overpeck, J.T., Otto-Bliesner, B., Heil, C.W., King, J., Scholz, C.A., Peck, J., 2015. The time-transgressive termination of the African Humid Period. Nat. Geosci. 8, 140–144. http://dx.doi.org/10.1038/ngeo2329.

Solmon, F., Mallet, M., Elguindi, N., Giorgi, F., Zakey, A., Konaré, A., 2008. Dust aerosol impact on regional precipitation over western Africa, mechanisms and sensitivity to absorption properties. Geophys. Res. Lett. 35, L24705. http://dx.doi.org/10.1029/2008GL035900.

Sultan, B., Janicot, S., 2003. The West African monsoon dynamics. Part II: the "preonset" and "onset" of the summer monsoon. J. Climate 16, 3407–3427. http://dx.doi.org/10.1175/1520-0442(2003)016<3407:TWAMDP>2.0.CO;2.

Taylor, K.E., Stouffer, R.J., Meehl, G.A., 2009. A summary of the CMIP5 experiment design. http://cmip-pcmdi.llnl.gov/cmip5/docs/Taylor_CMIP5_design.pdf.

Tegen, I., Hollrig, P., Chin, M., Fung, I., Jacob, D., Penner, J., 1997. Contribution of different aerosol species to the global aerosol extinction optical thickness: estimates from model results. J. Geophys. Res. 102, 23895. http://dx.doi.org/10.1029/97JD01864.

Texier, D., de Noblet, N., Braconnot, P., 2000. Sensitivity of the African and Asian monsoons to mid-Holocene insolation and data-inferred surface changes. J. Climate 13, 164–181. http://dx.doi.org/10.1175/1520-0442(2000)013<0164:SOTAAA>2.0.CO;2.

Valcke, S., 2006. OASIS3 user guide. PRISM Tech. Rep. 3. Partnership for Res. Infrastructures in Earth Syst. Model, Toulouse, France, 64 pp.

Vancoppenolle, M., Fichefet, T., Goosse, H., Bouillon, S., Madec, G., Morales Maqueda, M.A., 2008. Simulating the mass balance and salinity of Arctic and Antarctic sea ice. 1. Model description and validation. Ocean Model. http://dx.doi.org/10.1016/j.ocemod.2008.10.005.

Wang, C., Dong, S., Evan, A.T., Foltz, G.R., Lee, S.-K., 2012. Multidecadal covariability of North Atlantic sea surface temperature, African dust, Sahel rainfall, and Atlantic hurricanes. J. Climate 25, 5404–5415. http://dx.doi.org/10.1175/JCLI-D-11-00413.1.

Weldeab, S., Lea, D.W., Schneider, R.R., Andersen, N., 2007. 155,000 years of West African monsoon and ocean thermal evolution. Science 316, 1303–1307. http://dx.doi.org/10.1126/science.1140461.

Yoshioka, M., Mahowald, N.M., Conley, A.J., Collins, W.D., Fillmore, D.W., Zender, C.S., Coleman, D.B., 2007. Impact of desert dust radiative forcing on Sahel precipitation: relative importance of dust compared to sea surface temperature variations, vegetation changes, and greenhouse gas warming. J. Climate 20, 1445–1467. http://dx.doi.org/10.1175/JCLI4056.1.

Zhang, G., Cook, K.H., 2014. West African monsoon demise: climatology, interannual variations, and relationship to seasonal rainfall. J. Geophys. Res., Atmos. 119, 10,175–10,193. http://dx.doi.org/10.1002/2014JD022043.